frontiers | Frontiers in Energy Research

TYPE Brief Research Report
PUBLISHED 08 August 2022
DOI 10.3389/fenrg.2022.968259

Check for updates

OPEN ACCESS

EDITED BY
Zhen Li,
East China Jiaotong University, China

REVIEWED BY
Hangyu Zhou,
Tsinghua University, China
Wang Hongqiang,
Shandong University of Technology, China

*CORRESPONDENCE
Hong Zeng,
HongZeng@zju.edu.cn

SPECIALTY SECTION
This article was submitted to Electrochemical Energy Conversion and Storage, a section of the journal Frontiers in Energy Research

RECEIVED 13 June 2022
ACCEPTED 04 July 2022
PUBLISHED 08 August 2022

CITATION
Zeng H, He Y and Chamas M (2022), Si/Cu composite as anode material for lithium-ion batteries.
Front. Energy Res. 10:968259.
doi: 10.3389/fenrg.2022.968259

COPYRIGHT
© 2022 Zeng, He and Chamas. This is an open-access article distributed under the terms of the Creative Commons Attribution License (CC BY). The use, distribution or reproduction in other forums is permitted, provided the original author(s) and the copyright owner(s) are credited and that the original publication in this journal is cited, in accordance with accepted academic practice. No use, distribution or reproduction is permitted which does not comply with these terms.

Si/Cu composite as anode material for lithium-ion batteries

Hong Zeng[1,2]*, Yawen He[2] and Mohamad Chamas[2]

[1]College of Chemical and Biological Engineering, Zhejiang University, Hangzhou, China, [2]School of Chemistry and Chemical Engineering, Southwest Petroleum University, Chengdu, China

An Si/Cu composite anode was prepared using a facile solid mechanosynthesis method and wet chemical etching. Phase transition and morphologies were investigated on pristine and as-synthesized composites. Effects of presence of $Al_{80}Si_{20}$ and super *p* carbon on ball-milling were investigated. Moreover, the etching effect was compared with that of pristine Cu–Zn and composites by addition of NH_4Cl. The results of X-ray diffraction patterns, scanning-electron-microscopy morphological images, and focus-ion-beam/energy-dispersive mapping demonstrated that the formation of the intermetallic, elemental distribution, homogeneity, and dezincification is involved with the addition of Al, super *p* carbon, and etching additive NH_4Cl. Super *p* carbon avoided the formation of Cu–Si, while Al made the more homogenous distribution of Si/Cu. The two synthesized types of Si/Cu composites deliver specific capacity/retention rates of 608 $mAhg^{-1}$/66.4% (Si/Cu from pure Si) and 707 $mAhg^{-1}$/81.1% (Si/Cu from $Al_{80}Si_{20}$) after 200 cycles, respectively. The higher stability of the galvanostatic cycling and capability performance resulted from the homogeneity of Si and Cu.

KEYWORDS

Si/Cu, anode, lithium-ion battery, etching, mechanosynthesis

1 Introduction

The present commercial graphite delivers a theoretical capacity of 372 $mAhg^{-1}$, which could not meet the demand of high-capacity lithium-ion batteries. Si exhibits a theoretical capacity of 3580 $mAhg^{-1}$ ($Li_{3.75}Si$) (Zuo et al., 2017), so it is a promising anode material for lithium-ion batteries. Due to the volume expansion (>300%) of pure Si during lithiation/delithiation, Si has been fabricated to nanoscale particles, wires, and thin films (Maranchi et al., 2006; Polat et al., 2015), etc. On the other hand, conductive buffer or coating, such as Si/C (Chen et al., 2017), metal Si/Cu (Sethuraman et al., 2011), native oxides Si/SiO_x (Zheng et al., 2018), and transitional metal composites Si/Mxenes (Hui et al., 2019), could improve the stability of Si and increase the conductivity of the particles. Those strategies (Luo et al., 2018) have been proved to stabilize the electrochemical performance of the electrode. In this work, we are focusing on Si/Cu composite material because of high conductivity and malleability of Cu.

Ahn et al. (2006) used the co-sputtering method for preparing Si–Cu nanocomposite, which delivered a stable cycling performance of 400 $mAhg^{-1}$ over 40 cycles. The Cu nanodots were dispersed around the Si matrix. McDowell et al. (2012) prepared Cu coating on

the surface of crystal nanowire Si. The suppressed Li_xSi from Cu coating was observed using the *in situ* technique. But for a large-scale production, the solution method could make composites more controllable and dispersed with lower cost. However, the nano-scale Cu is easily oxidized by forming Cu_xO in the solution. For example, Jiang et al. (2017) used a reduction procedure, preparing Cu from Cu_2O. Li et al. (2015) synthesized Cu coating on Si through three steps. Therefore, a simplifying procedure is imperative for powder production. The mechanical milling method of synthesizing composite material is ideal for a large-scale production. The mechanical milling process would also decrease the particle size (Kasavajjula et al., 2007). For example, Si composites (Edfouf et al., 2013; Ladam et al., 2017) were fabricated using the Ar-protection ball-milling method. The size of Si particles obviously decreases, which is beneficial for cycling stabilization (Yang et al., 2002). During the ball milling process, the challenge is the excessive formation of the intermediate phases (Cu_xSi and SiC, etc.), which are electrochemically inactive and decrease the capacity of the electrode. Al Bacha et al. (2020) reported the effect of additives on the ball milling process of alloys and investigated on elemental distribution and performance, etc. The incorporation effect (Ma et al., 2010) is discussed when adding additives in the ball milling process.

In this work, the composite is mixed with the micro-scale powder, such as Cu–Zn alloy, Si, or Al–Si. The as-synthesized composites were compared with the addition of Al and super *p* carbon in mechanical ball milling. Then, the effect of the additive (NH_4Cl) in etching solution was compared with that of pristine Cu–Zn and as-synthesized composites. The purpose of this study was to simplify the method for synthesizing Si/Cu composite anode materials. Afterward, the morphology, elemental distribution, and Li storage performance/stability were investigated between the synthesized Si/Cu composites.

2 Experimental

2.1 Synthesis

First, the micro-scale Si powder (micro-Si "MS" or $Al_{80}Si_{20}$ "AS"), micro-scale Cu–Zn powder (CZ), and super *p* (C) were thoroughly mixed using a mortar inside the glove box (filled with argon 99.999%) and then placed in a high-energy ball milling for 48 h to obtain a precursor (500 rpm, 8 balls, ss316L pots, powder: balls = 16:1). Furthermore, 2 g of the as-synthesized powder was added to 2.0M HCl solution (room temperature) or a mixed acid solution of 2.0M HCl and 5.0M NH_4Cl (70°C under N_2 flow) for dealloying, respectively. The etching process was maintained for 2–5°h. Afterward, the mixture was filtered and repeatedly washed with deionized water and ethanol. Finally, the obtained powder was dried in a vacuum oven at 60° C overnight.

2.2 Characterization

X-ray diffraction (XRD) is a method for analyzing the phase composition and crystal structure of a sample. XRD was carried out using an X-Pert PRO machine (Malvern Panalytical) under CuKa radiation λ = 0.154056 nm. The temperature was 21°C, and the humidity was 55%. The prepared composite powder was analyzed by scanning electron microscopy (SEM) using an FEI Inspect F50 apparatus. Elemental analysis was carried out by energy dispersive X-ray spectroscopy (EDS) using field emission scanning electron microscopy (FESEM) FEI Inspect F50 with accelerating voltage in the range from 200 V to 30 kV.

2.3 Electrochemistry

The working electrodes were prepared by mixing 80 wt% of composite, 10 wt% of sodium carboxymethyl-cellulose (Na-CMC, M_w 250,000), and 10 wt% of super *p* in 2 ml deionized water for 3 h. We prepared uniform slurry (450 rpm, 3 balls, ss304L pots) with a proper amount of deoxidized water in high-energy ball milling and applied it to the current collector copper foil. The thickness was 60 mm. We then placed the coated copper foil into a vacuum drying oven. It was dried in a vacuum for 2 h. The dried sample was taken out and punched with a hole puncher having a diameter of 12 mm to obtain the electrode disk. The electrochemical measurements were performed in Li half coin-cells assembled in the argon glove box (<0.1 ppm O_2 and H_2O). The electrolyte was 1 M $LiPF_6$ (EC/DMC, 1:1, v/v) with 10 wt% FEC and 2 wt% VC. A glass fiber GF/D was used as a separator. The coin-cell CR2032 was in the galvanostatic with a voltage cut-off of 0.05–1.2 V using the Neware battery test system. The active mass of the cycled electrodes is approximately 1.0 mg.

3 Results and discussion

Figure 1A shows the XRD patterns of all raw materials. By comparing Jade software with the standard diffraction pattern database, it can be seen that the peaks located at 28.4°, 47.3°, and 56.1° reflect the (111), (220), and (311) crystal planes of Si (JCPDS no. 27–1402) in the patterns of micro-Si and $Al_{80}Si_{20}$, respectively. The peaks at 38.5° and 44.7° are in accordance with the (111) and (200) crystal planes of Al (JCPDS no. 85–1327), respectively. No other intermediate phase peaks were found. The weaker peak intensity and broadening of Si of $Al_{80}Si_{20}$ is related to the less Si amount and smaller crystalline size. By Scherrer's equation (Shibata et al., 2008), the Si crystalline sizes of micro-Si and $Al_{80}Si_{20}$ are 58 and 10 nm, respectively. The Cu–Zn micro-powder consists of two phases: $Cu_{0.64}Zn_{0.36}$ (JCPDS no. 50–1333) and CuZn (JCPDS no. 02–1231), which is similar to Zhang et al. (2019). The sharp and well-crystalline peak at 42.3° and 49.5° are

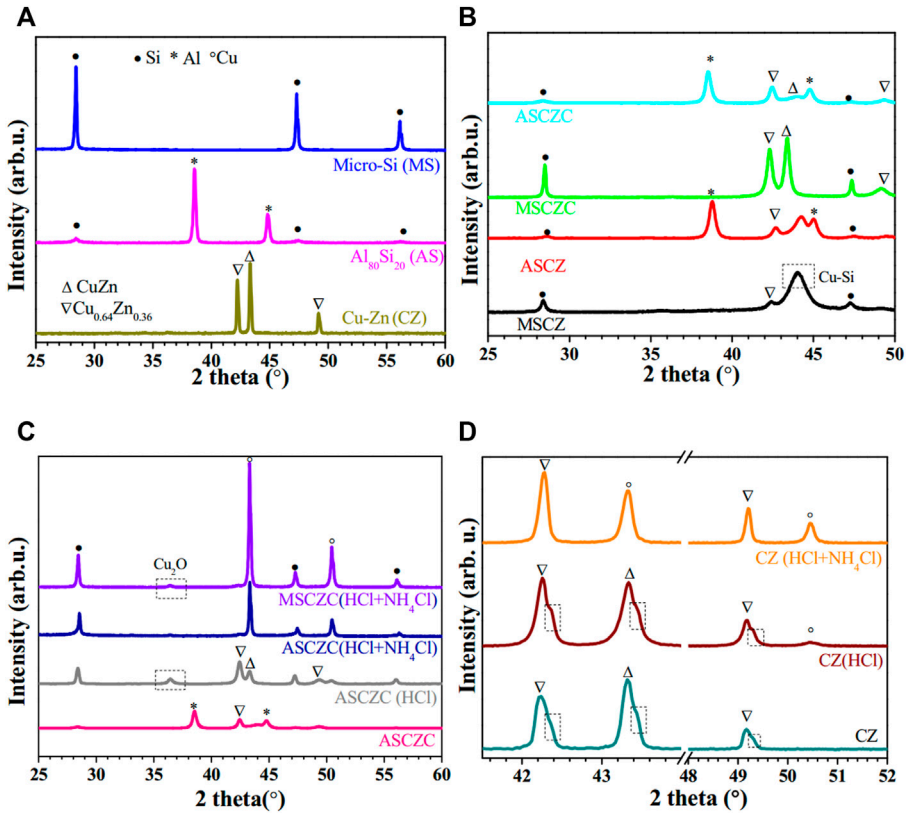

FIGURE 1
XRD patterns of **(A)** raw powder, **(B)** as-synthesized composites, **(C)** composites after the etching process (by HCl and HCl/NH_4Cl, respectively), and **(D)** Cu–Zn alloy before and after etching.

assigned to planes (111) and (200) of $Cu_{0.64}Zn_{0.36}$, respectively. In addition, the peaks of Cu–Zn at 43.5° should be attributed to the crystal plane (110) of CuZn. All those raw materials were used as powder precursors, and the mixture was directly ball-milled under protection of Ar.

The powder mixture was divided into two criteria, with and without Al or SP, to investigate the effect during the ball milling synthesis. In Figure 1B, the mass ratios of the as-synthesized composites are typically as follows: MS/CZ (25/75), AS/CZ (55/45), MS/CZ/C (25/65/10), and AS/CZ/C (55/40.6/4.4). The initial mass ratio was to fix Si with a mass ratio of 25% after etching (removing Zn and Al). For MSCZ, the broadening and large peak at 44° is assigned to Cu–Si and Cu–Zn alloy, which consumes the active Si. This phenomenon is not observed in ASCZ. The peaks of Cu–Zn at 42.6° and 44.2° are typically shifted and broadened. Meanwhile, the intensity decrease of CuZn and $Cu_{0.64}Zn_{0.36}$ could be due to Cu–Zn amorphization. The possible reason could be the presence of Al.

In MSCZ, there is a broadening peak at 44° that is possibly from the Cu_xSi formation (Meng et al., 2016). In MSCZC and ASCZC, the crystalline peaks for both Si and Cu–Zn are broadened, which is due to the mechanical effect from ball milling. For ASCZC, the crystals Si, Al, and $Cu_{0.64}Zn_{0.36}$ were typically shown. Therefore, the Cu–Si was prohibited by addition of super *p* carbon, which could be attributed to the lubricant effect from carbon (Al Bacha et al., 2020).

In Figure 1C, it is shown that the etching solution contains 2.0M HCl. Al was successfully removed which can be seen from the absence of Al peaks in ASCZC. However, Cu_2O was observed at 36.4°. Zn still exists as Cu–Zn, while Cu peaks locate at 43.3° and 50.4°. With the addition of 5 M NH_4Cl to 2.0M HCl, Cu peaks are observed in both ASCZC and MSCZC. Meanwhile, the formation of crystal Cu_2O is prohibited in the ASCZC. It could be concluded that Si/Cu was obtained by MSCZC or ASCZC with the mixed etching solution of 2.0M HCl and 5.0M NH_4Cl. However, partial dezincification was observed in the pristine micro-scale Cu–Zn particle by the etching solution in Figure 1D. Shoulder peaks located at 42.3°, 43.5°, and 49.3° are corresponding to $Cu_{0.64}Zn_{0.36}$ and CuZn phases in CZ (HCl). Cu peaks could be seen in CZ (HCl + NH_4Cl), while the main peaks of $Cu_{0.64}Zn_{0.36}$ and CuZn were maintained. This phenomenon suggests that the dezincification is involved with particle size of Cu–Zn. Ball

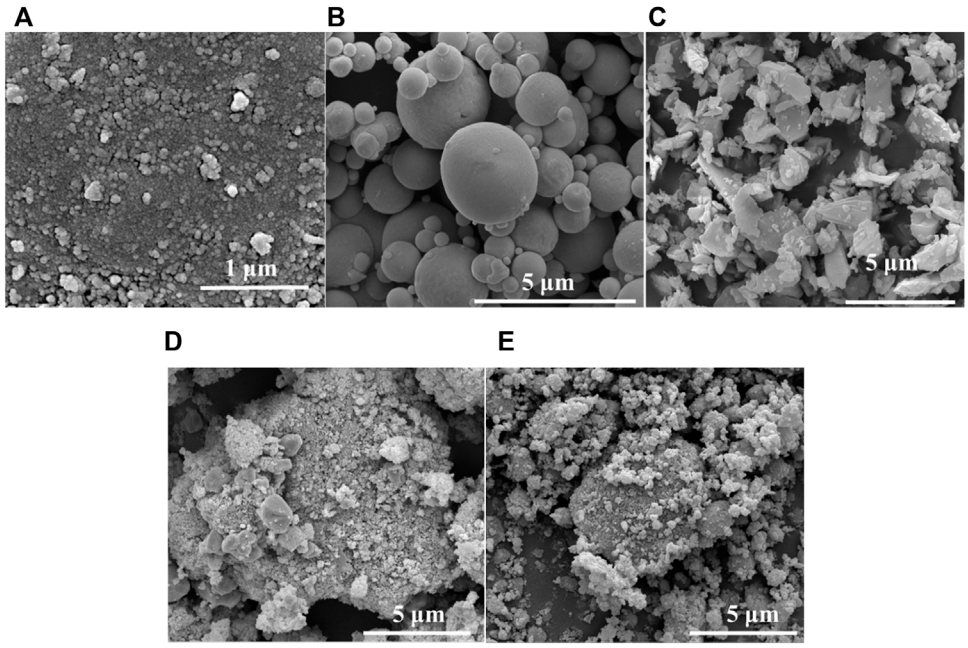

FIGURE 2
SEM of **(A)** raw powder micro-scale Cu-Zn, **(B)** $Al_{80}Si_{20}$, and **(C)** micro-Si and as-synthesized Si/Cu composite prepared by **(D)** micro-Si and **(E)** $Al_{80}Si_{20}$.

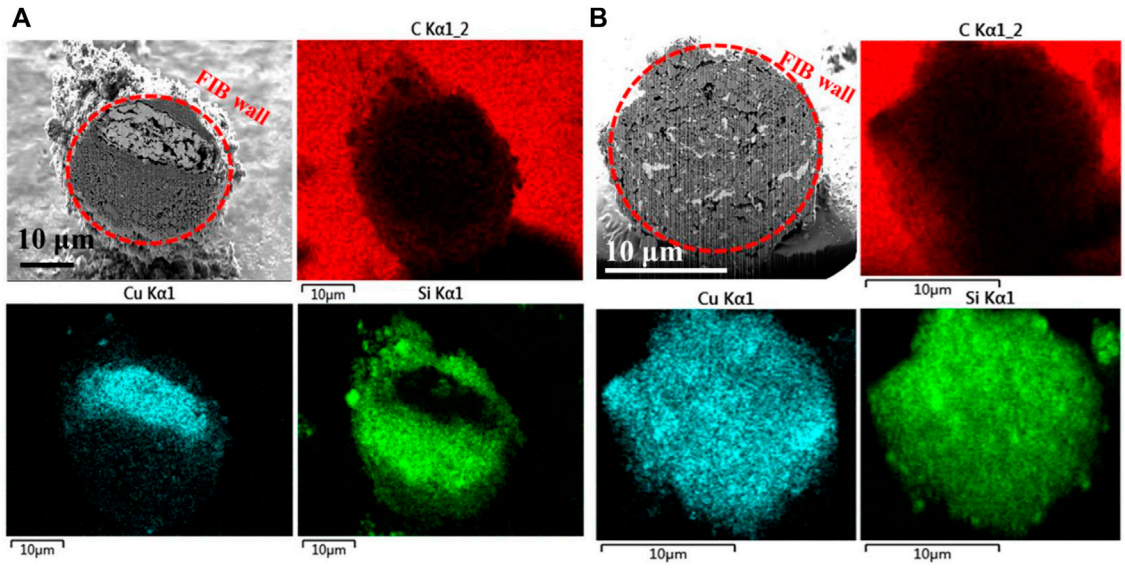

FIGURE 3
FIB-SEM images of as-synthesized Si/Cu composites prepared from **(A)** micro-Si and **(B)** $Al_{80}Si_{20}$.

milling could decrease the particle size, which explains the dezincification of the ball-milled composite.

Figure 2 exhibits the structure of raw material and synthesized composites. Cu–Zn (Figure 2A) and $Al_{80}Si_{20}$ (Figure 2B) show micro-scale spherical particles. Micro-Si (Figure 2C) shows disordered rock-like structures. Figure 2D and Figure 2E are the Si/Cu composites, which suggest a similar structure but unknown element distribution.

The expected composition is a well-dispersed Si and Cu. From the FIB-SEM-EDS mapping images (Figure 3), the Si/Cu

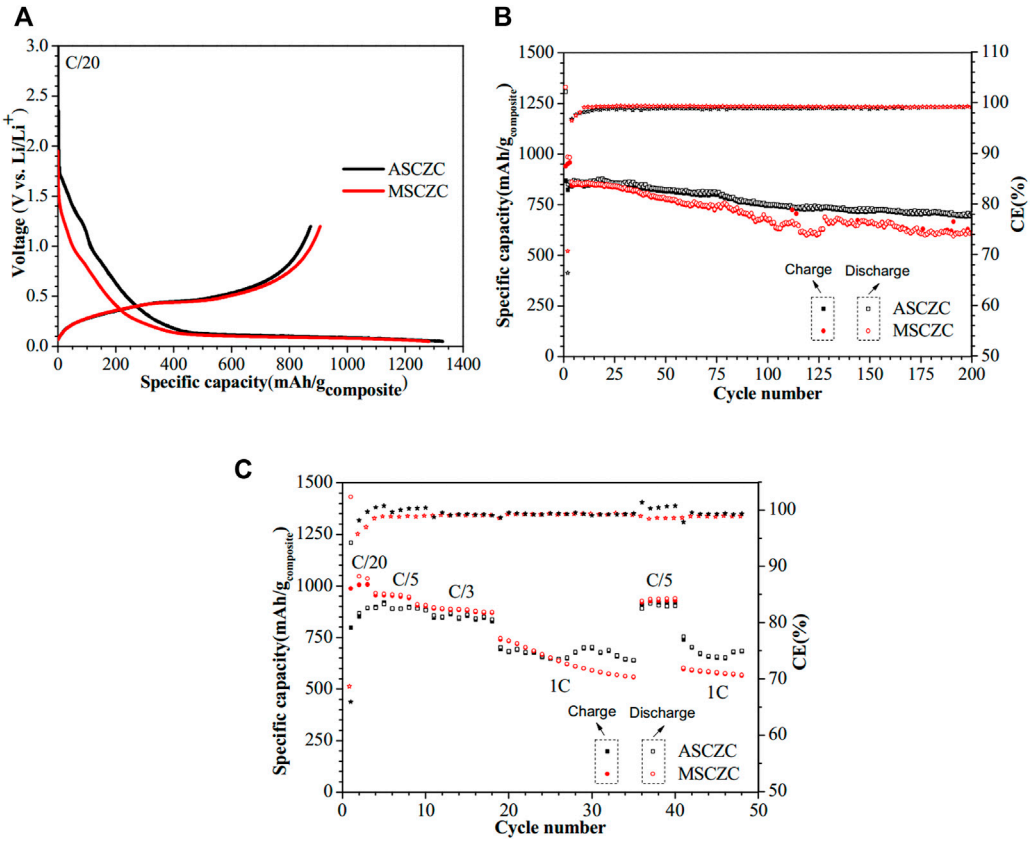

FIGURE 4
Electrochemical **(A)** voltage profiles at C/20, **(B)** cycling performance at C/5, and **(C)** C-rate capability performance of Si/Cu composites.

TABLE 1 Comparison between previously published works on Si/Cu composite anode materials for Li-ion batteries and the present results.

Composition	Si precursor and synthesis method	Capacity retention (%)	Cycling performance
Cu/Si Ahn et al. (2006)	Si, thin film, co-sputtering method	54	400 $mAhg^{-1}$ at the 40th cycle
Cu/Si Sethuraman et al. (2011)	Si, 500 nm film, sputtering deposition	77	2002 $mAhg^{-1}$ at the 50th cycle
Flat Cu/Si Moon et al. (2018)	Si sputtering target, sputtering deposition	42.9	978 $mAhg^{-1}$ at the 100th cycle
Porous Cu/Si Moon et al. (2018)	Si sputtering target, sputtering deposition	63.4	1321 $mAhg^{-1}$ at the 100th cycle
Cu/Si (this work)	Al–Si powder, low-speed ball milling and chemical etching	81.1	707 $mAhg^{-1}$ at the 200th cycle

composite prepared by micro-Si and Cu–Zn shows a core–shell structure. The core is Cu, with a Si shell. On the other hand, the composite prepared by $Al_{80}Si_{20}$ and Cu–Zn shows a homogenous elemental distribution and dispersive Si/Cu. The possible explanation could be the initial particle size and morphology. More ordered morphology of $Al_{80}Si_{20}$ contributes to the homogeneity of the composite.

The voltage profile of those two types of Si/Cu composites is exhibited in Figure 4A. During the first lithiation, the first plateau at a voltage of 0.8 V is due to the SEI formation. The Li consumption of 0.7–0.25 V could be ascribed to the lithiation of surface oxides. Typically, a plateau is observed at ~1.5 V in ASCZC/Li. This is the characteristic lithiation of Cu_2O (Grugeon et al., 2001). ASCZC and MSCZC show specific capacities of 1330/872 $mAhg^{-1}$ and 1281/916 $mAhg^{-1}$ of first discharge/charge, respectively. The values are consistent with the extra Cu_2O reaction.

In Figure 4B, the electrodes were discharged/charged for three cycles at a rate of C/20. The following cycle rate is C/5. The Coulombic efficiency of MSCZC and ASCZC increases from 71 to 96% and 66 to 97% for the two first cycles, respectively. Then, there is a gradual increase up to 99% for the following three cycles and a stabilization at this value until the end of cycling. The retention rate is 66.4% (MSCZC) and 81.1% (ASCZC) after 200 cycles, respectively. The higher cycling stability of ASCZC/Li could be due to the homogeneity of the composition and smaller Si size. Compared with other Si/Cu electrode materials, the currently synthesized composites have low but much stable capacities, which are reflected in the significantly higher capacity retention (Table 1). In Figure 4C, it could be seen that ASCZC shows a better capability c-rate performance by comparing the specific capacity difference: 960 (C/20)/958 (C/5)/906 (C/3)/700 (1C) $mAhg^{-1}$ for ASCZC and 980 (C/20)/906 (C/5)/840 (C/3)/586 (1C) $mAhg^{-1}$ for MSCZC, respectively. The stabilized capacity value at different rates should be ascribed to the conductivity to the connection of composite particles (Zhang et al., 2018).

4 Conclusion

In this work, mechanical ball-milling using micro-scale Cu–Zn, $Al_{80}Si_{20}$, and pure Si and one-step HCl/NH_4Cl etching were applied for preparing Si/Cu composites as anode material for lithium-ion batteries. Presence of super *p* carbon could prohibit the formation of electrochemically inactive Cu–Si during ball-milling. On the other hand, Si/Cu synthesized from $Al_{80}Si_{20}$ exhibited a better homogeneity. The addition of NH_4Cl promoted dezincification of the Cu–Zn in the composite, which was after ball-milling. The partial dezincification was observed for the pristine Cu–Zn micro-scale powder, which suggests the importance of composite size. Moreover, Si/Cu (ASCZC) exhibits a more stable electrochemical galvanostatic cycling, capability, and performance than the Si/Cu (MSCZC). The Si-based anode material has a high theoretical specific capacity, and this work will provide certain insights into the subsequent porous Si-based composites.

Data availability statement

The original contributions presented in the study are included in the article/Supplementary Material; further inquiries can be directed to the corresponding author.

Author contributions

HZ synthesized Si/Cu materials, performed physical and electrochemical characterizations, and revised this manuscript. YH performed data analysis and drafted and edited the manuscript. MC, who provided guidance on materials and electrochemistry, contributed to the quality of this manuscript with his knowledge and many discussions.

Funding

This work was funded by the National Natural Science Foundation of China under Grant No. 21650110463, the PHC XU GUANGQI 2017 (38796XG) Program, and the Southwest Petroleum University Key Project (KSZ16083).

Conflict of interest

The authors declare that the research was conducted in the absence of any commercial or financial relationships that could be construed as a potential conflict of interest.

Publisher's note

All claims expressed in this article are solely those of the authors and do not necessarily represent those of their affiliated organizations, or those of the publisher, the editors, and the reviewers. Any product that may be evaluated in this article, or claim that may be made by its manufacturer, is not guaranteed or endorsed by the publisher.

References

Ahn, H.-J., Kim, Y.-S., Kim, W. B., Sung, Y.-E., and Seong, T.-Y. (2006). Formation and characterization of Cu–Si nanocomposite electrodes for rechargeable Li batteries. *J. Power Sources* 163, 211–214. doi:10.1016/j.jpowsour.2005.12.077

Al Bacha, S., Zakhour, M., Nakhl, M., and Bobet, J.-L. (2020). Effect of ball milling in presence of additives (graphite, $AlCl_3$, $MgCl_2$ and NaCl) on the hydrolysis performances of $Mg_{17}Al_{12}$. *Int. J. Hydrogen Energy* 45, 6102–6109. doi:10.1016/j.ijhydene.2019.12.162

Chen, H., Hou, X., Qu, L., Qin, H., Ru, Q., Huang, Y., et al. (2017). Electrochemical properties of core-shell nano-Si@carbon composites as superior anode materials for high-performance Li-ion batteries. *J. Mat. Sci. Mat. Electron.* 28, 250–258. doi:10.1007/s10854-016-5518-x

Edfouf, Z., Fariaut-Georges, C., Cuevas, F., Latroche, M., Hézèque, T., Caillon, G., et al. (2013). Nanostructured $Ni_{3.5}Sn_4$ intermetallic compound: An efficient buffering material for Si-containing composite anodes in lithium ion batteries. *Electrochim. Acta* 89, 365–371. doi:10.1016/j.electacta.2012.11.078

Grugeon, S., Laruelle, S., Herrera-Urbina, R., Dupont, L., Poizot, P., Tarascon, J.-M., et al. (2001). Particle size effects on the electrochemical performance of copper oxides toward lithium. *J. Electrochem. Soc.* 148, A285. doi:10.1149/1.1353566

Hui, X., Zhao, R., Zhang, P., Li, C., Wang, C., Yin, L., et al. (2019). Low-temperature reduction strategy synthesized Si/Ti_3C_2 MXene composite anodes for high-performance Li-ion batteries. *Adv. Energy Mat.* 9, 1901065. doi:10.1002/aenm.201901065

Jiang, J., Lim, Y. S., Park, S., Kim, S.-H., Yoon, S., Piao, L., et al. (2017). Hollow porous Cu particles from silica-encapsulated Cu_2O nanoparticle aggregates effectively catalyze 4-nitrophenol reduction. *Nanoscale* 9, 3873–3880. doi:10.1039/c6nr09934c

Kasavajjula, U., Wang, C., and Appleby, A. J. (2007). Nano- and bulk-silicon-based insertion anodes for lithium-ion secondary cells. *J. Power Sources* 163, 1003–1039. doi:10.1016/j.jpowsour.2006.09.084

Ladam, A., Bibent, N., Cénac-Morthé, C., Aldon, L., Olivier-Fourcade, J., Jumas, J.-C., et al. (2017). One-pot ball-milling synthesis of a Ni-Ti-Si based composite as anode material for Li-ion batteries. *Electrochim. Acta* 245, 497–504. doi:10.1016/j.electacta.2017.05.093

Li, C., Zhang, P., and Jiang, Z. (2015). Effect of nano Cu coating on porous Si prepared by acid etching Al-Si alloy powder. *Electrochimica Acta* 161, 408–412. doi:10.1016/j.electacta.2015.02.087

Luo, Z., Xu, J., Yuan, B., Hu, R., Yang, L., Gao, Y., et al. (2018). 3D hierarchical porous Cu-based composite current collector with enhanced ligaments for notably improved cycle stability of Sn anode in Li-ion batteries. *ACS Appl. Mat. Interfaces* 10, 22050–22058. doi:10.1021/acsami.8b04049

Ma, Q.-C., Zhang, G.-J., Kan, Y.-M., Xia, Y.-B., and Wang, P.-L. (2010). Effect of additives introduced by ball milling on sintering behavior and mechanical properties of hot-pressed B_4C ceramics. *Ceram. Int.* 36, 167–171. doi:10.1016/j.ceramint.2009.07.014

Maranchi, J. P., Hepp, A. F., Evans, A. G., Nuhfer, N. T., and Kumta, P. N. (2006). Interfacial properties of the a-Si/Cu: Active-inactive thin-film anode system for lithium-ion batteries. *J. Electrochem. Soc.* 153, A1246. doi:10.1149/1.2184753

McDowell, M. T., Lee, S. W., Wang, C., and Cui, Y. (2012). The effect of metallic coatings and crystallinity on the volume expansion of silicon during electrochemical lithiation/delithiation. *Nano Energy* 1, 401–410. doi:10.1016/j.nanoen.2012.03.004

Meng, Y., Ma, F., Song, Z. X., Li, Y. H., and Xu, K. W. (2016). Nano-grained ZrB_2 thin films as a high-performance diffusion barrier in Cu metallization. *RSC Adv.* 6, 844–850. doi:10.1039/C5RA20864E

Moon, S.-H., Kim, S.-J., Kim, M.-C., So, J.-Y., Lee, J.-E., Shin, Y.-K., et al. (2018). Stress-relieved Si anode on a porous Cu current collector for high-performance lithium-ion batteries. *Mat. Chem. Phys.* 223, 152–156. doi:10.1016/j.matchemphys.2018.10.042

Polat, B. D., Eryilmaz, O. L., Keleş, O., Erdemir, A., and Amine, K. (2015). Compositionally graded SiCu thin film anode by magnetron sputtering for lithium ion battery. *Thin Solid Films* 596, 190–197. doi:10.1016/j.tsf.2015.09.085

Sethuraman, V., Kowolik, K., and Srinivasan, V. (2011). Increased cycling efficiency and rate capability of copper-coated silicon anodes in lithium-ion batteries. *J. Power Sources* 196, 393–398. doi:10.1016/j.jpowsour.2010.06.043

Shibata, T., Fukuda, K., Ebina, Y., Kogure, T., and Sasaki, T. (2008). One-nanometer-thick seed layer of unilamellar nanosheets promotes oriented growth of oxide crystal films. *Adv. Mat.* 20, 231–235. doi:10.1002/adma.200701381

Yang, J., Takeda, Y., Imanishi, N., Capiglia, C., Xie, J. Y., and Yamamoto, O. (2002). SiOx-based anodes for secondary lithium batteries. *Solid State Ionics* 152-153, 125–129. doi:10.1016/S0167-2738(02)00362-4

Zhang, D., Dai, A., Wu, M., Shen, K., Xiao, T., Hou, G., et al. (2019). Lithiophilic 3D porous CuZn current collector for stable lithium-metal batteries. *ACS Energy Lett.* 5, 180–186. doi:10.1021/acsenergylett.9b01987

Zhang, X., Ou-Yang, W., Zhu, G., Lu, T., and Pan, L. (2018). Shuttle-like carbon-coated FeP derived from metal-organic frameworks for lithium-ion batteries with superior rate capability and long-life cycling performance. *Carbon* 143, 116–124. doi:10.1016/j.carbon.2018.11.005

Zheng, G., Xiang, Y., Xu, L., Luo, H., Wang, B., Liu, Y., et al. (2018). Controlling surface oxides in Si/C nanocomposite anodes for high-performance Li-ion batteries. *Adv. Energy Mat.* 8, 1801718. doi:10.1002/aenm.201801718

Zuo, X., Zhu, J., Müller-Buschbaum, P., and Cheng, Y.-J. (2017). Silicon based lithium-ion battery anodes: A chronicle perspective review. *Nano Energy* 31, 113–143. doi:10.1016/j.nanoen.2016.11.013